This article has been accepted for publication in a future issue of this journal, but has not been fully edited. Content may change prior to final publication. Citation information: DOI 10.1109/TMAG.2021.3091522, IEEE Transactions on Magnetics

Simultaneous Evaluation of Permeability and Permittivity using a Flexible Microstrip Line-Type Probe up to 67 GHz

S. Yabukami[1,2] *Member, IEEE*, C. Iwasaki[1], K. Nozawa[2], S. Takahashi[3], K. Okita[1], K. Chatani[4]

[1] Graduate School of Biomedical Engineering, Tohoku University, Sendai 980-8579, Japan
[2] Graduate School of Engineering, Tohoku University, Sendai 980-8579, Japan
[3] Department of Electrical, Information and Physics Engineering, Tohoku University, Sendai 980-8579, Japan
[4] Tokin Corporation, Sendai 982-8510, Japan

Complex relative permeability and permittivity were evaluated simultaneously in the band of 100 MHz–67 GHz using a flexible microstrip line-type probe. In principle, the probe can evaluate the permeability and permittivity of electromagnetic materials regardless of size. The measured permeability and permittivity were obtained from the transmission coefficient (S_{21}). Since S_{21} under the infinite magnetic field can be estimated by changing the DC magnetic field stepwise, the magnetic and dielectric signals were separated accurately. The complex permeability and permittivity of an NiZn ferrite sheet (10 mm × 10 mm, 0.1 mm thick) and polytetrafluoroethylene (PTFE) (25 mm × 25 mm, 0.79 mm thick) were evaluated accurately.

***Index Terms*—Complex relative permeability measurement, permittivity measurement, microstrip line-type probe, sample size limitation**

I. INTRODUCTION

The development of various devices and systems for 5G, beyond 5G, etc. is underway, and research and development of materials for electromagnetic wave absorbers, noise suppressors, and electromagnetic shields covering several tens of GHz bands is also advancing. Demand for high-frequency permeability and permittivity evaluation of electromagnetic materials is increasing because high-frequency electromagnetic materials have both permeability and permittivity. There are several methods to evaluate the permeability and permittivity of electromagnetic materials simultaneously. In the coaxial probe method, the sample must be processed into a solenoid shape and narrow bandwidth [1]. In the Nicolson-Ross-Weir method, problems such as narrow frequency band and sample size limitation arise [2]. Further, in the harmonic resonance cavity perturbation method, it is necessary to process the sample into a special shape such as a needle shape and measurement frequency is single or restrictive [3]. In measurement by transmission in free space, the method has disadvantages of requiring a large sheet as the sample and low sensitivity [4].

In our previous work, we developed a flexible microstrip line-type probe, and presented permeability measurement of magnetic thin film [5]. This probe comprises a transmission line, and, since the traveling wave electromagnetic field propagates, the electromagnetic field changes regarding both the dielectric and the magnetic material. Therefore, we considered this probe applicable not only to permeability evaluation, but also to permittivity evaluation.

In this study, this probe simultaneously evaluates permittivity and permeability of electromagnetic materials without restriction on sample size. First, we developed a wideband flexible microstrip probe. Next, the permittivity of a dielectric material (non-magnetic material) was evaluated. Finally, the complex permeability and complex permittivity of an NiZn ferrite sheet, which has both magnetism and dielectricity, were evaluated up to 67 GHz. The advantage of this method is that magnetic permeability and permittivity can be measured in an ultra-wideband up to 67 GHz regardless of sample size. The drawbacks of this method are that the electric and magnetic fields on the sample are not uniform and the average physical characteristic constants are measured.

Manuscript received March 17, 2021. Corresponding author: S. Yabukami (e-mail: yab@ecei.tohoku.ac.jp).

II. EXPERIMENT SETUP

2.1 New probe and system setup

Figures 1(a) and 1(b) show schematic views of the microstrip line-type probe. Figure 1(c) shows a photograph of the probe. The probe consists of a microstrip conductor (0.36 mm wide) on a flexible substrate (RT/duroid® 5870), a ground plane, lead lines, and two K (2.92 mm) coaxial connectors. The microstrip conductor has a flexible substrate and a straight portion and a tapered portion. The straight portion of the microstrip conductor is close to the

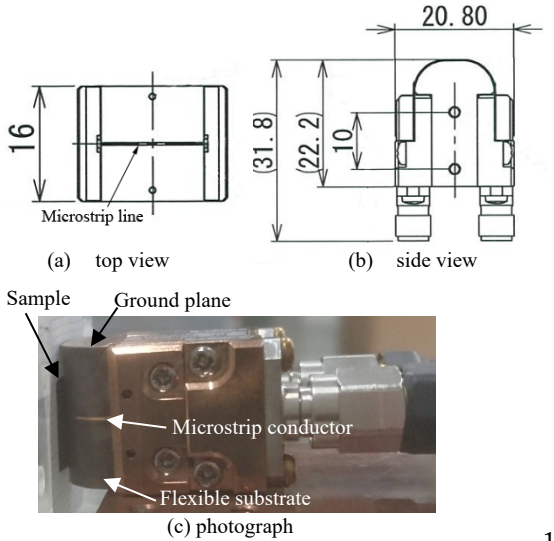

Fig. 1 Schematic and photographic views of the probe.

This article has been accepted for publication in a future issue of this journal, but has not been fully edited. Content may change prior to final publication. Citation information: DOI 10.1109/TMAG.2021.3091522, IEEE Transactions on Magnetics

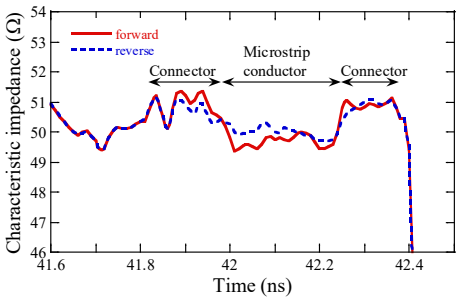

Fig. 2 Characteristic impedance of the probe measured by time-domain reflectometry (TDR).

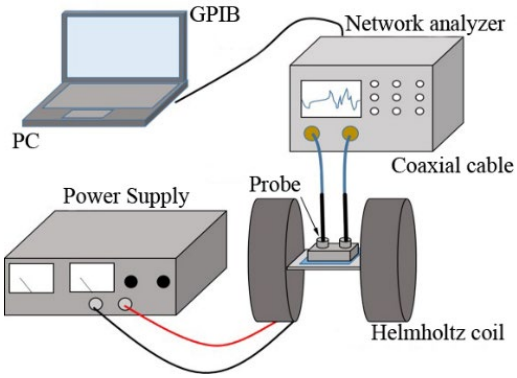

Fig. 3 Schematic diagram of setup for measuring permeability and permittivity.

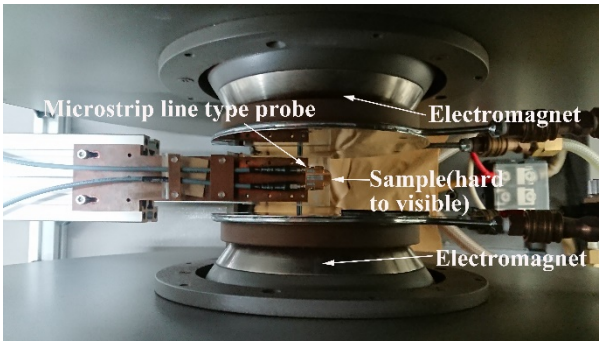

Fig. 4 Photograph of the probe and setup.

sample. Since the microstrip line slopes, large samples can be placed in close proximity. Figure 2 shows the characteristic impedance of the probe measured using time-domain reflectometry (N5227A). The characteristic impedance was 49.5 Ω–50.5 Ω along the microstrip line in proximity with the sample, and 49.5 Ω – 51.5 Ω along the total probe including the K coaxial connectors. Since the probe has a flexible substrate, it can be evaluated with a high SN ratio by directly attaching a sample with low permeability or low permittivity. Figure 3 shows the system setup, which consists of the probe, a Helmholtz coil, network analyzer (Agilent Technologies N5227A), DC power supply, and personal computer. Coaxial cables are connected to the network analyzer. Figure 4 shows a photograph of the probe arrangement, sample, coaxial cables, and electromagnet. The electromagnet applies a DC magnetic field to the sample, whose direction is perpendicular to the RF magnetic field. The system setup resembled those used in earlier studies [5]. The electromagnetic sample was in direct contact with the microstrip conductor in this work.

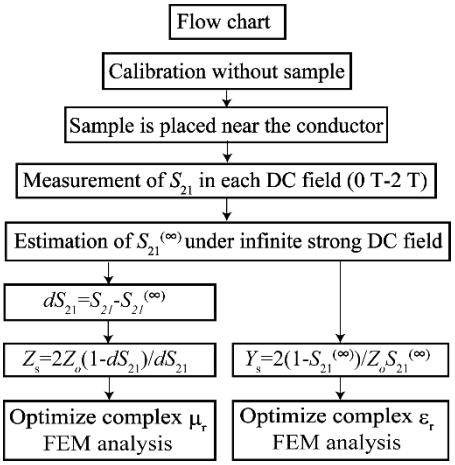

Fig. 5 Flow chart of permeability and permittivity measurements.

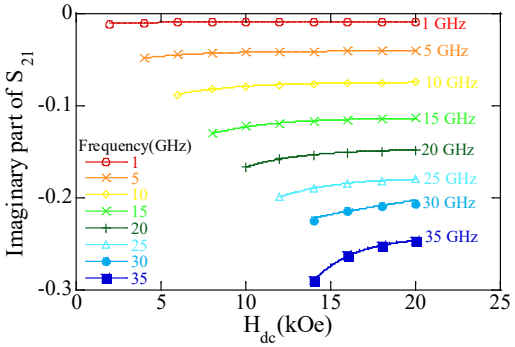

Fig. 6 Optimization of $S_{21}^{(\infty)}$.

2.2 Optimization of permeability and permittivity

Figure 5 presents a flow chart to obtain permeability and permittivity. First, S_{21} is calibrated without the sample. Secondly, the sample is set close to the microstrip conductor. S_{21} is measured in each DC field when the DC field (0 T, 0.2 T,···, 2 T) is applied using the electromagnet. Thirdly, from the change in S_{21} when each DC magnetic field was applied, $S_{21}^{(\infty)}$ is estimated when an infinite magnetic field is applied. Figure 6 shows the process to obtain the imaginary part of $S_{21}^{(\infty)}$ as a function of the applied field up to 35 GHz. In Fig. 6, when the DC magnetic field is strengthened, S_{21} gradually approaches a constant value. This curve was approximated by the least square method using the exponential function of Eq. (1).

$$S_{21} = C_1 + C_2 \times e^{(-C_3 H_{dc})} \quad (1)$$

Where C_1, C_2, C_3 is constant, C_1 was defined as $S_{21}^{(\infty)}$. At frequencies above 35 GHz, it overlapped with ferromagnetic resonance in a strong magnetic field of around 1.5 - 2 T. In this case, as the relative permeability without the DC field nearly equaled $1 - j0$ above 35 GHz, $S_{21}^{(\infty)}$ was obtained asymptotically from S_{21} of the low magnetic field ($H_{dc} = 0$). The real part of S_{21} was also obtained using this method. Since $S_{21}^{(\infty)}$ represents the state in which the magnetic signal of the sample is removed, the relative permeability and the permittivity can be separated. The complex impedance and admittance are calculated using Eq. (2) and (3), respectively.

$$Z_s = 2Z_o(1 - dS_{21})/dS_{21} \quad (2)$$

This article has been accepted for publication in a future issue of this journal, but has not been fully edited. Content may change prior to final publication. Citation information: DOI 10.1109/TMAG.2021.3091522, IEEE Transactions on Magnetics

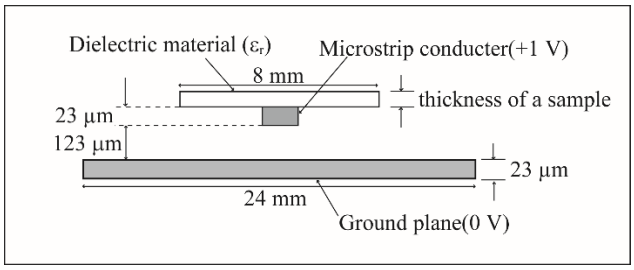

Fig. 7 Electric field calculation model by FEM analysis.

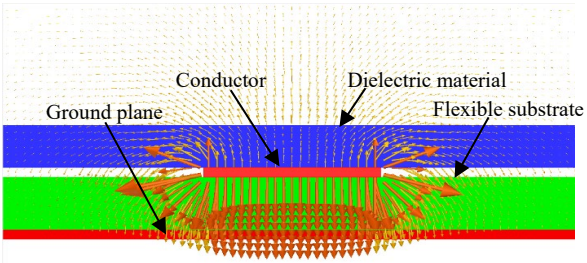

Fig. 8 Electric field distribution of the cross-sectional model.

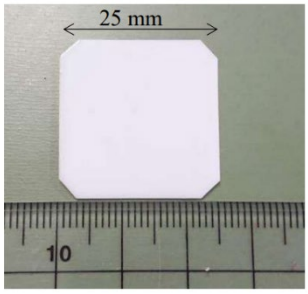

Fig. 9 Photograph of the polytetrafluoroethylene (PTFE) (25 mm × 25 mm, 0.79 mm thick).

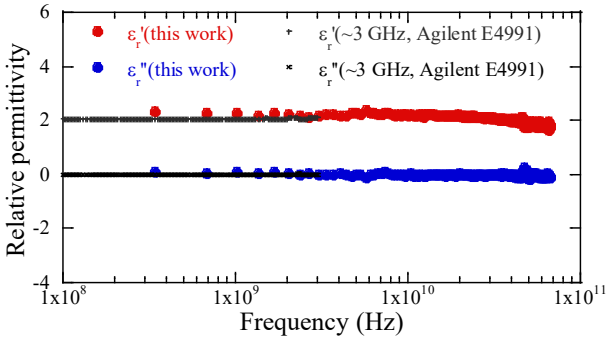

Fig. 10 Complex permittivity of the polytetrafluoroethylene (PTFE) (25 mm × 25 mm, 0.79 mm thick).

$$Y_s = 2(1 - dS_{21})/Z_o S_{21} \quad (3)$$

Equations (2) and (3) are derived from transmission line theory by placing the contribution of the sample with series impedance element Z_s or admittance Y_s [6]. Z_o shows the characteristic impedance, and dS_{21} and Z_s or Y_s include multiple reflections in Eq. (2) and (3).

The complex permeability or permittivity of the sample is obtained using finite element method (FEM) analysis. Figure 7 shows the electric field calculation model and a cross-sectional view of the microstrip line and a sample. Input voltage was applied to the microstrip conductor and ground plane. The electric field was calculated using FEM analysis (Maxwell 2D, Ansoft Co.). The calculated capacitance was obtained from the electric field integral.

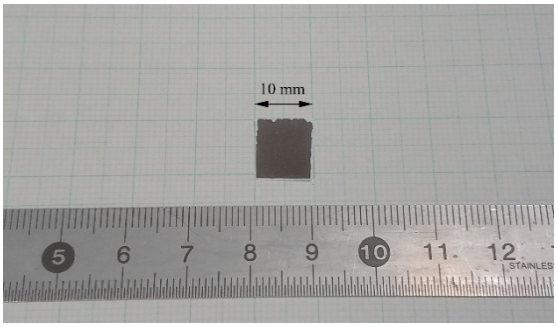

Fig. 11 Photograph of the NiZn ferrite sheet (10 mm × 10mm, 0.1mm thick).

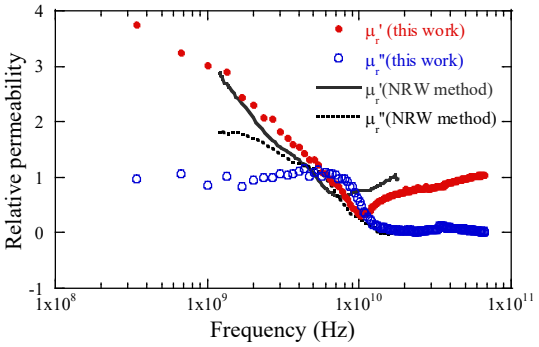

Fig. 12 Relative permeability of the NiZn ferrite sheet (10 mm × 10 mm, 0.1 mm thick).

The relative permittivity of the sample was changed from 1 to 1000 as a parameter. Figure 8 presents the electric field of the cross-sectional model at 1 GHz with dielectric material for a relative permittivity of 10. The relationship between the relative permittivity and the capacitance is obtained from electric field analysis by the finite element method. The real part of the relative permittivity is optimized from the measured value of the capacitance obtained from Eq. (3) and the finite element method analysis [7]. The imaginary part of the relative permittivity, ε_r", was obtained from the ratio of the measured susceptance to conductance. In optimizing permeability, the relationship between inductance and permeability was calculated by the finite element method (magnetic field analysis). Using this, the permeability was obtained from the measured inductance. The imaginary part of the relative permeability, μ_r", was obtained from the ratio of resistance to reactance [5].

III. EXPERIMENT RESULTS

3.1 Permittivity of the polytetrafluoroethylene (PTFE)

Figure 9 shows a photograph of the polytetrafluoroethylene (PTFE), which is 25 mm x 25 mm and 0.79 mm thick. The PTFE is a dielectric standard material. The sample is not a magnetic material, so a DC magnetic field is not necessary. The measurement results of the complex relative permittivity are shown in Fig. 10. The relative permittivity was about 2.2, and the results showed good agreement with the reference measured by using Agilent E4991A (~3 GHz) [8]. The error was calculated using Eq. (4), and the maximum error was about 9% up to 3 GHz. Therefore, it is considered that the permittivity can be measured accurately by this method.

This article has been accepted for publication in a future issue of this journal, but has not been fully edited. Content may change prior to final publication. Citation information: DOI 10.1109/TMAG.2021.3091522, IEEE Transactions on Magnetics

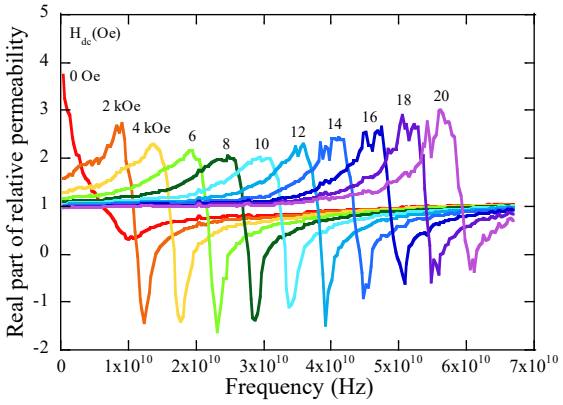

(a) real part

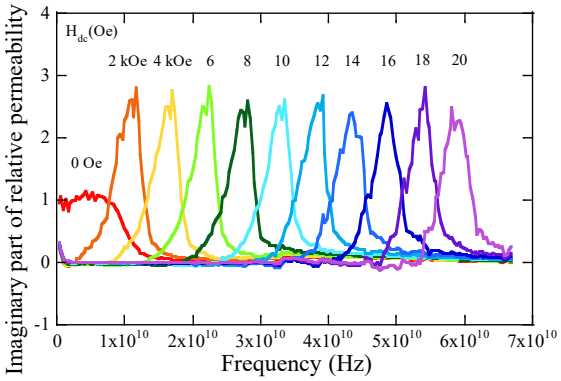

(b) imaginary part

Fig. 13 Relative permeability of the NiZn ferrite sheet (10 mm × 10 mm, 0.1 mm thick), when bias DC magnetic field is applied (0 T ⋯2 T).

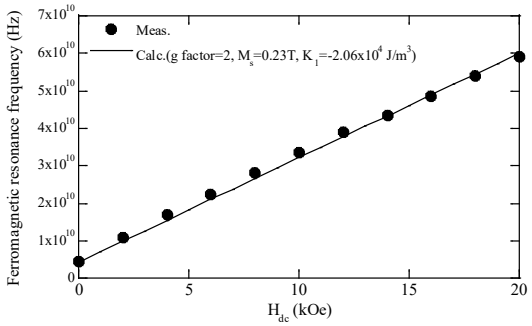

Fig. 14 Ferromagnetic resonance frequency as a function of applied DC field (45 mm × 25 mm, 0.5 μm thick).

$$Error = \frac{\varepsilon_r - \varepsilon_r^{(ref)}}{\varepsilon_r^{(ref)}} \quad (4)$$

3.2 NiZn ferrite sheet

Figure 11 shows a photograph of the NiZn ferrite sheet. The permeability and permittivity of the NiZn ferrite sheet were measured using the method in Section 2.2. This sample comprises NiZn ferrite (JFE Steel Corp., KNI-106 [10]) mixed at 52 vol% and hardened with epoxy. The film thickness is about 100 μm. Figure 12 shows the relative permeability of the NiZn ferrite sheet evaluated by this method, which was compared with the Nicolson-Ross-Weir method (1-18 GHz) [2]. The reference sample had a ring shape (7 mm in outer diameter, 3 mm in inner diameter, and 0.432 mm in thickness). Both measured values roughly corresponded, demonstrating the validity of this method. The measurement error of permeability, μ_r', was up to 50% in the range of 1 GHz–8 GHz. The error in the band above 8 GHz and μ_r" under 4 GHz was assumed to be the demagnetizing effect that comes from the difference in the driving magnetic field between the proposed method and Nicolson-Ross-Weir method. Correction considering the demagnetizing effect will be undertaken in the next paper.

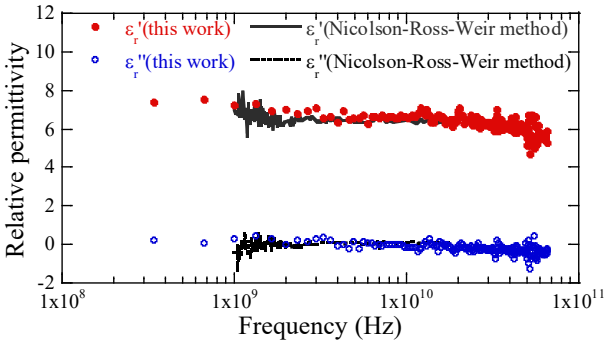

Fig. 15 Relative permittivity of the NiZn ferrite sheet (10 mm × 10 mm, 0.1 mm thick).

Figure 13 shows the measured permeability when a DC field of 0 T–2 T is applied. Figure 13 (a) shows the real part and (b) shows the imaginary part. When the DC magnetic field was increased, the ferromagnetic resonance frequency shifted to the high-frequency side. On the other hand, we have already reported that the imaginary part of permeability became negative in the high-frequency range because of insufficient saturation of 2 T [9]. In this study, the problem that the imaginary part becomes negative has been roughly resolved by the estimation of $S_{21}^{(\infty)}$ under the infinite magnetic field. Figure 14 shows the ferromagnetic resonance frequency as a function of the applied DC magnetic field. The measured resonance frequency came from Fig. 13, and the theoretical resonance frequency was obtained from LLG equations [11]. The measured ferromagnetic resonance frequency agreed well with the theoretical frequency. Error was within 6% from no bias field to 20 kOe. Therefore, the method is applicable for very wideband measurements up to 67 GHz.

The measurement results of permittivity are shown in Fig. 15. As shown in Fig. 5, permittivity was obtained from $S_{21}^{(\infty)}$ with estimation of the infinite magnetic field, and it is considered that the magnetic signal and the dielectric signal could be separated by this method. The permittivity was about 6.5 in the low frequency, which agreed well with the Nicolson-Ross-Weir method (1–18 GHz) [2]. The error was calculated using Eq. (4), and the error was within 5% from 3 GHz–18 GHz except for noisy frequency bands. In the frequency band of about 50 GHz or higher, as the reflection microwave at the material becomes large, it is considered that the measurement error increases with S_{21} alone.

IV. CONCLUSIONS

We have developed a broadband simultaneous evaluation system for complex permeability and

permittivity of electromagnetic materials. The magnetic field was changed stepwise to estimate S_{21} under an infinite magnetic field, and the magnetic signal and the dielectric signal were separated using the proposed method. A polytetrafluoroethylene (PTFE) (25 mm × 25 mm, 0.79 mm thick) and a NiZn ferrite sheet (10 mm × 10 mm, 0.1 mm thick) were evaluated in the band of 100 MHz–67 GHz. Their measured permeability and permittivity showed rough agreement with other methods.

ACKNOWLEDGMENTS

This work was supported in part by the Business Incubation Program (BIP) of Tohoku University, and in part by research and development for expansion of radiowave resources from the Ministry of Internal Affairs and Communications (JPJ000254).

REFERENCES

[1]https://www.keysight.com/jp/ja/assets/7018-03896/brochures/5991-2171.pdf

[2] A. M. Nicolson and G. F. Ross, *IEEE Trans. Instrum. Meas*., Vol. 19, 377–382 (1970).

[3] T. Miura, K. Tahara, and M. Horibe, *Proc. Asia-Pacific Microwave Conference*, TH2C-1 (2014).

[4] C.G. Montgomery, "Technique of Microwave Measurements," pp. 593, McGraw-Hill Book Company (1947).

[5] S. Yabukami, K. Nozawa, L. Tonthat, K. Okita, and S. Ranajit, *IEEE Tran. Magnetics*, Vol. 56, 6100405 (2020).

[6] A. Smith, "Radio Frequency Principles and Applications," 157 (New York: IEEE Press, 1998).

[7] K. Ikeda, N. Kobayashi, K. I. Arai, and S. Yabukami, *Journal of Magnetism and Magnetic Materials*, Vol. 446, p. 80 (2018).

[8] Keysight Technologies Selection Guide, p. 50 (2015).

[9] S. Yabukami, K. Nozawa, L. Tonthat, K. Okita, M. Sato, and S. Sugimoto, *The Annual Conference of Magnetic Materials and Magnetism 2020*, H4-03 (2020).

[10] JFE TECHNICAL REPORT, 26, 77 (2010).

[11] S. Chikazumi, "Physics of Ferromagnetism", p. 324 (1984).